Journal of the Korean Ceramic Society
Vol. 40, No. 11, pp. 1047~1057, 2003.

Review Article

Scanning Nonlinear Dielectric Microscopy : Overview - A High Resolution Tool for Observing Ferroelectric Domains and Nano-domain Engineering -

Yasuo Cho†

Research Institute of Electrical Communication, Tohoku University, 2-1-1 Katahira, Aoba-ku, Sendai 980-8577, Japan

(Received October 16, 2003; Accepted November 18, 2003)

ABSTRACT

A sub-nanometer resolution Scanning Nonlinear Dielectric Microscope (SNDM) was developed for observing ferroelectric polarization. We also demonstrate that the resolution of SNDM is higher than that of a conventional piezo-response imaging. Secondly, we report new SNDM technique detecting higher nonlinear dielectric constants ε_{3333} and ε_{33333}. Higher order nonlinear dielectric imaging provides higher lateral and depth resolution. Finally, the formation of artificial small inverted domain is reported to demonstrate that SNDM system is very useful as a nano-domain engineering tool. The nano-size domain dots were successfully formed in $LiTaO_3$ single crystal. This means that we can obtain a very high density ferroelectric data storage with the density above 1T-bits/inch^2.

Key words : Scanning nonlinear dielectric microscope, Ferroelectri polarization

1. Introduction

Recently, ferroelectric materials, especially in thin film form, have attracted the attention of many researchers. Their large dielectric constants make them suitable as dielectric layers of microcapacitors in microelectronics. They are also investigated for application in nonvolatile memory using the switchable dielectric polarization of ferroelectric material. To characterize such ferroelectric materials, a high-resolution tool is required for observing the microscopic distribution of remanent (or spontaneous) polarization of ferroelectric materials.

With this background, we have proposed and developed a new purely electrical method for imaging the state of the polarizations in ferroelectric and piezoelectric material and a their crystal anisotropy. It involves the measurement of point-to-point variations of the nonlinear dielectric constant of a specimen and is termed " Scanning Nonlinear Dielectric Microscopy (SNDM)".[1-7] This is the first successful purely electrical method for observing the ferroelectric polarization distribution without the influence of the screening effect from free charges. To date, the resolution of this microscope has been improved down to the sub-nanometer order.

Here we describe the theory for detecting polarization and the technique for nonlinear dielectric response and report the results of the imaging of the ferroelectric domains in single crystals and thin films using SNDM. Especially in a measurement of PZT thin film, it was confirmed that the resolution was sub-nanometer order. We also describe the theoretical resolution of SNDM. Moreover, we demonstrate that the resolution of SNDM is higher than that of a conventional piezo-response imaging by using Scanning Force Microscopy (SFM) technique.[8,9]

Next, we report new SNDM technique. In the above conventional SNDM technique, we measure the lowest order nonlinear dielectric constant ε_{333}, which is a 3rd rank tensor. To improve the performance and resolution of SNDM, we have modified the technique such that higher nonlinear dielectric constants ε_{3333}(4th rank tensor), ε_{33333} (5th rank tensor) are detected. It is expected that higher order nonlinear dielectric imaging will provide higher lateral and depth resolution. We confirmed this improvement over conventional SNDM imaging experimentally, and used the technique to observe the growth of a surficial paraelectric layer on periodically poled $LiNbO_3$.[10-12]

Finally, the formation of artificial small inverted domain is reported to demonstrate that SNDM system is very useful as a nano-domain engineering tool. The nano-size domain dots were successfully formed in $LiTaO_3$ single crystal. This means that we can obtain a very high density ferroelectric data storage with the density above T-bits/inch^2.

2. Nonlinear Dielectric Imaging with Sub-nanometer Resolution

First, we briefly describe the theory for detecting polarization. Precise descriptions of the principle of the microscope

†Corresponding author : Yasuo Cho
E-mail : cho@riec.tohoku.ac.jp
Tel : +81-22-217-5529 Fax : +81-22-217-5529

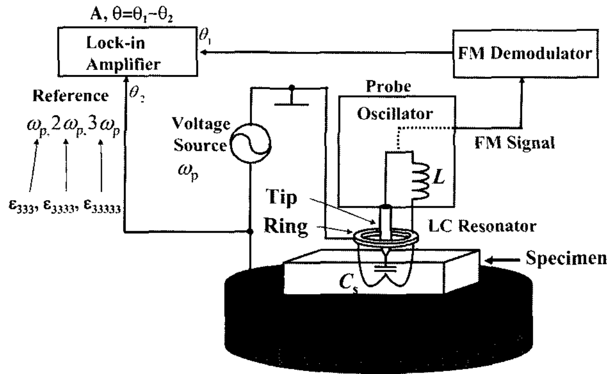

Fig. 1. Schematic diagram of SNDM.

have been reported elsewhere (see refs. 3,4). We also report the results of the imaging of the ferroelectric domains in single crystals and in thin films using the SNDM. Especially in the PZT thin film measurement, we succeeded to obtain a domain image with a sub-nanometer resolution.

2.1. Principle and Theory for SNDM

Fig. 1 shows the system setup of the SNDM using the LC lumped constant resonator probe.[4] In the figure, $C_s(t)$ denotes the capacitance of the specimen under the center conductor (the tip) of the probe. $C_s(t)$ is a function of time because of the nonlinear dielectric response under an applied alternating electric field $E_{p3}(=E_p\cos\dot{u}_p t,\ f_p=5-100\ \text{kHz})$. The ratio of the alternating variation of capacitance $\Delta C_s(t)$ to the static value of capacitance C_{s0} without time dependence is given as[3]

$$\frac{\Delta C_S(t)}{C_{s0}} = \frac{\varepsilon_{333}}{\varepsilon_{33}} E_p \cos\omega_p t + \frac{\varepsilon_{3333}}{4\varepsilon_{33}} E_p^2 \cos 2\omega_p t \quad (1)$$

where ε_{33} is a linear dielectric constant and ε_{333} and ε_{3333} are nonlinear dielectric constants. The even rank tensor, including the linear dielectric constant ε_{33}, does not change with 180° rotation of the polarization. On the other hand, the lowest order of the nonlinear dielectric constant ε_{333} is a third-rank tensor, similar to the piezoelectric constant, so that there is no ε_{333} in a material with a center of symmetry, and the sign of ε_{333} changes in accordance with the inversion of the spontaneous polarization.

This LC resonator is connected to the oscillator tuned to the resonance frequency of the resonator. The above mentioned electrical parts (*i.e.* tip, ring, inductance, and oscillator) are assembled into a small probe for the SNDM. The oscillating frequency of the probe (or oscillator) (around 1.3 GHz) is modulated by the change of capacitance $\Delta C_s(t)$ due to the nonlinear dielectric response under the applied electric field. As a result, the probe (oscillator) produces a Frequency Modulated (FM) signal. By detecting this FM signal using the FM demodulator and lock-in amplifier, we obtain a voltage signal proportional to the capacitance variation. Each signal corresponding to ε_{333} and ε_{3333} was obtained by setting the reference signal of the lock-in amplifier at the frequency ω_p of the applied electric field and at the doubled frequency $2\omega_p$, respectively. Thus we can detect the nonlinear dielectric constant just under the needle and can obtain the fine resolution determined by the diameter of the pointed end of the tip and the linear dielectric constant of specimens. The capacitance variation caused by the nonlinear dielectric response is quite small ($\Delta C_s(t)/C_{s0}$ is in the range from 10^{-3} to 10^{-8}.). Therefore the sensitivity of SNDM probe must be very high. The measured value of the sensitivity of an above mentioned lumped constant probe is 10^{-22} F.

2.2. Nonlinear Dielectric Imaging

The tip of the lumped constant resonator probe was fabricated using electrolytic polishing of a tungsten wire or a metal coated conductive cantilever. The radius of curvature of the chip was 1 mm−25 nm. To check the performance of the new SNDM, first, we measured the macroscopic domains in a multidomain $BaTiO_3$ single crystal. Fig. 2 shows the two-dimensional image of the so called 90° a-c domain which is obtained by a coarse scanning over a large area. The sign of the nonlinear dielectric constant ε_{333} of the +c-domain is negative, whereas it is positive in the -c-domain. Moreover the magnitude of $\varepsilon_{111}=\varepsilon_{222}$ is zero in the a-domain, because $BaTiO_3$ belongs to tetragonal system at room temperature. Thus, we can easily distinguish the type of the domains.

To demonstrate that this microscopy is also useful for the domain measurement of thin ferroelectric films, we measured a PZT thin film. Fig. 3 shows the SNDM (a) and AFM (b) images taken from a same location of PZT thin film deposited on a $SrTiO_3$ (STO) substrate using metal organic chemical vapor deposition.

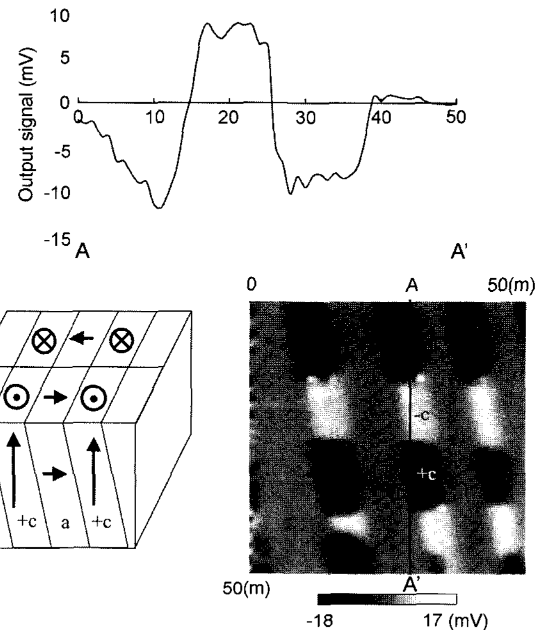

Fig. 2. A two-dimensional image of the 90° a-c domain in a $BaTiO_3$ single crystal and the cross-sectional (one-dimensional) image along the line A-A'.

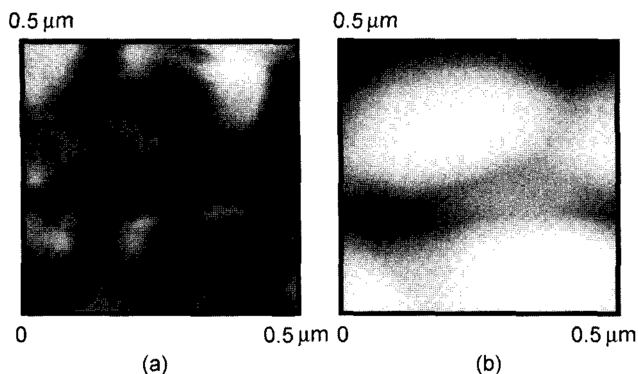

Fig. 3. Images of a PZT film on a $SrTiO_3$ substrate. (a) Domain patterns by SNDM and (b) surface morphology by AFM.

From the figure, it is apparent that the film is polycrystalline (from Fig. 3(b)) and that each grain in the film is composed of a several domains (from Fig. 3(a)). From X-ray diffraction analysis, this PZT film belongs to the tetragonal phase and the diffraction peaks, corresponding to both the c-axis and a-axis, were observed. Moreover, in Fig. 3(a), the observed signals were partially of zero amplitude, and partially positive. Thus, the images show that we succeeded in observing 90° a-c domain distributions in a single grain of the film.

These images of the film were taken from a relatively large area. Therefore, we also tried to observe very small domains in the same PZT film on STO substrate. The results are shown in Fig. 4(a) and 4(b). The bright area and the dark area correspond to the negative polarization and the positive polarization, respectively. It shows that we can successfully observe a nano-scale 180° c-c domain structure. Fig. 4(b) shows a cross sectional image taken along line A-A' in Fig. 4(a). As shown in this figure, we measured the c-c domain with the width of 1.5 nm. Moreover we fined that the resolution of the microscope is less than 0.5 nm.

However, as the above mentioned data shown in Fig. 4 was phase images, some readers may think that the sub-nanometer resolution of SNDM is not convincingly proven in the references because phase profiles are invariably abrupt and can not be considered as the definition of the resolution and amplitude signals show more realistic resolution. Therefore, here, we show the amplitude (A cosθ) images in Fig. 5 to demonstrate the resolution of SNDM is really sub-nanometer order. These images were taken from a epitaxial PZT thin (4000 Å)/La-Sr-Co-O/$SrTiO_3$.[13] The macroscopic surface topography and the domain pattern of this PZT thin film are shown in Fig. 6. Square c-domains and their surrounding a-domain strip pattern are clearly observed.

The strip shape domain pattern is seen in Fig. 5 (which is a magnified image of Fig. 6). Fig. 5(b) is a cross sectional image taken along line A-A' in Fig. 5(a). From the distance between the clearly distinguishable structures in the image, it is apparent that SNDM has sub-nanometer resolution.

To clarify the reason why such high resolution can be eas-

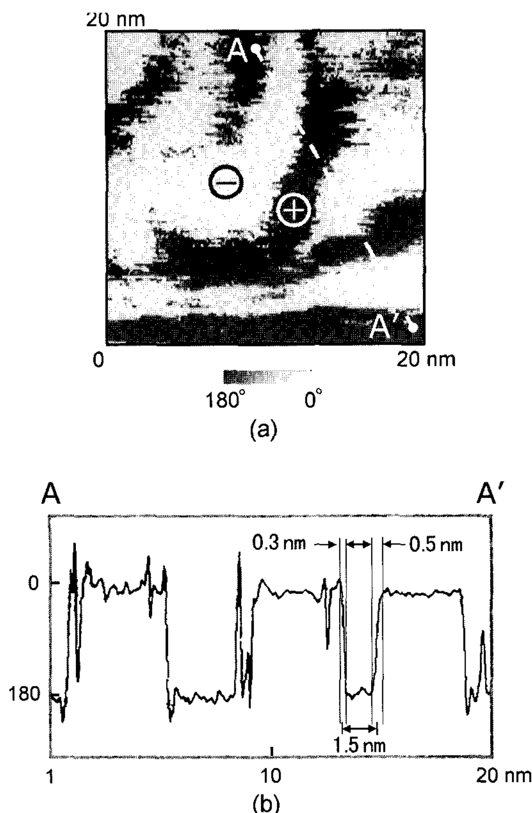

Fig. 4. Nano-scale ferroelectric domain on PZT thin film, (a) domain image and (b) cross-sectional (one-dimensional) image of phase signal along the line A-A'.

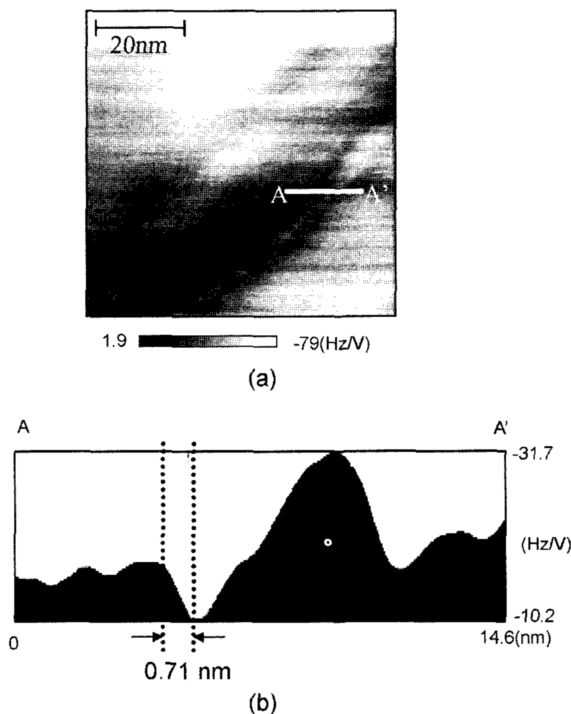

Fig. 5. (a) amplitude image of nanoscale ferroelectric domain on PZT thin film and (b) cross-sectional amplitude image taken along A-A'.

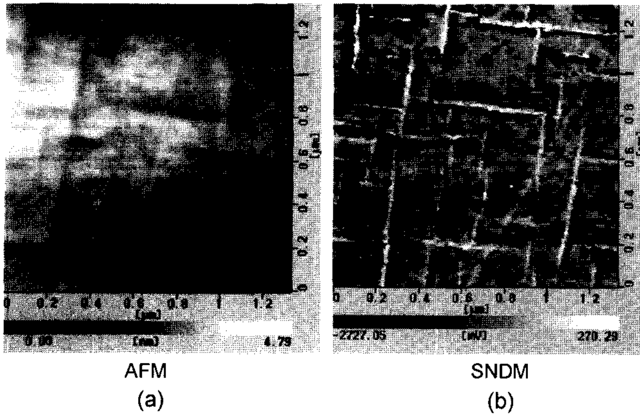

Fig. 6. Macroscopic surface topography and domain pattern taken from a epitaxial PZT thin (4000 Å)/La-Sr-Co-O/$SrTiO_3$.

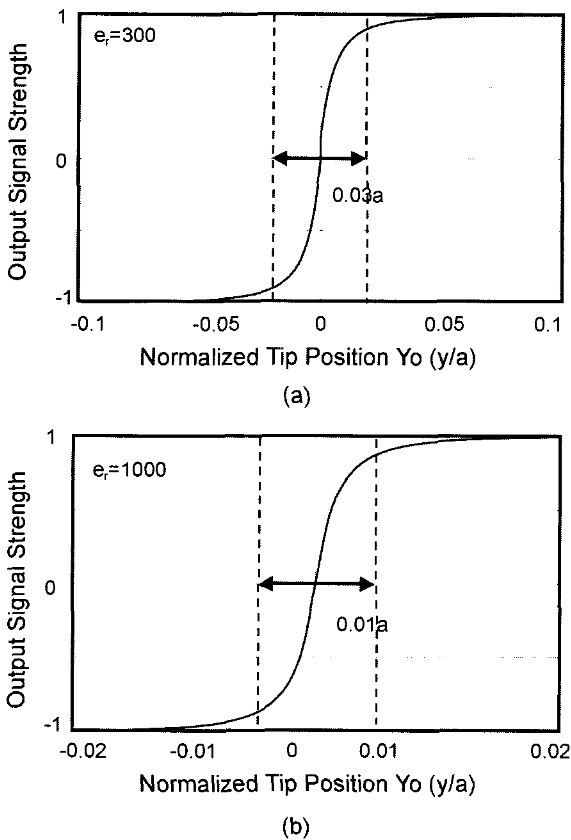

Fig. 7. Theoretical images of the 180° c-c domain boundary.

ily obtained, even if a relatively thick needle is used for the probe, we show the calculated results of the one dimensional image of 180° c-c domain boundary lying at y=0 (We chose y direction as the scanning direction).[14,15] Fig. 7 shows the calculated results where Y_0 is the tip position normalized with respect to the tip radius a. The resolution of the SNDM image is heavily dependent on the dielectric constant of the specimen. For example, for the case of $\varepsilon_{33}/\varepsilon_0$=1000 and a=10 nm, an atomic scale image will be able to be taken by SNDM.

2.3. Comparison between SNDM Imaging and Piezo-Response Imaging

Another frequently reported high-resolution tool for observing ferroelectric domains is piezoelectric response imaging using SFM.[8,9] From the viewpoint of resolution for ferroelectric domains, SNDM will surpass the piezo-response imaging because SNDM measures the nonlinear response of a dielectric material which is proportional to the square of the electric field, whereas the piezoelectric response is linearly proportional to the electric field. The concentration of the distribution of the square of the electric field in the specimen underneath the tip is much higher than that of the linear electric field. Thus, SNDM can resolve smaller domains than that measured by piezo-imaging technique. To prove this fact experimentally, we also performed the simultaneous measurements of the same location of the above mentioned PZT film sample by using AFM (topography)-, SNDM-, and piezo-imaging. The result is shown in Fig. 8. These domain images were taken under identical conditions except that the applied voltage was 2Vpp in the SNDM imaging and 8Vpp in the piezo-imaging. In the both SNDM image and piezo image, large negative signal was observed on the ñc-domain and almost zero signal was detected on the a-domain, because there is a crystal symmetry along the depth direction on the a-domain. Form the images, we can prove that SNDM can resolve greater detail than a conventional piezo-response imaging by using SFM technique.

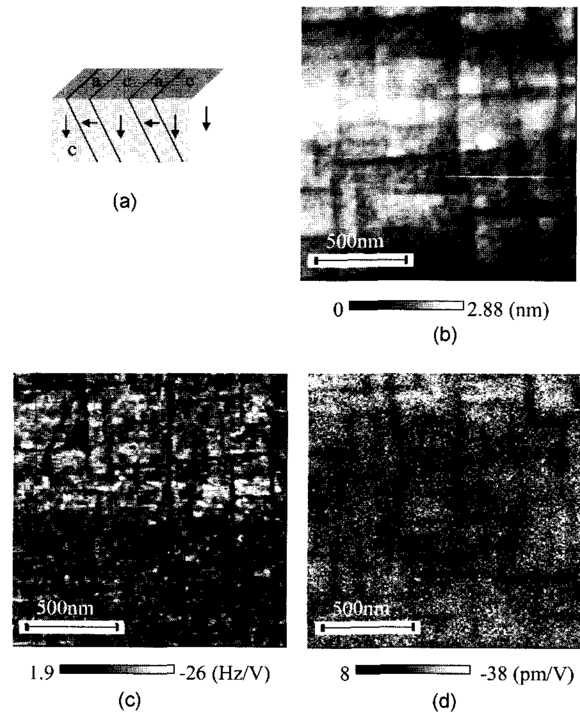

Fig. 8. Simultaneously taken images of a PZT film; (a) schematic domain structure (b) topography by AFM, (c) domain patterns by SNDM, and (d) domain patterns by SFM (piezo-imaging).

2.4. Observation of Domain Walls in PZT Thin Film Using SNDM

Several studies have examined the thickness of the domain wall in ferroelectric materials.[16] The 90° a-c domain wall thickness has been measured using a Transmission Electron Microscope (TEM),[13] but distinguishing the positive and negative domains in 180° opposite polarization areas is difficult because these methods are used to observe the strain of arrangements of molecules. Direct clarification of the domain wall thickness is important with respect to both scientific and engineering aspects.

Therefore we observed the 90° a-c domain walls and the 180° c-c domain walls in the above mentioned same epitaxial PZT thin film grown on $SrTiO_3$ using SNDM.

The linear dielectric constant of a-domain is expected to be larger than that of c-domain based on the $BaTiO_3$ single crystal analogy. To the author's knowledge, no actual observation of linear dielectric constant of a- and c-domains in PZT has been reported. Because obtaining a PZT single crystal of sufficient size in order to compare the linear dielectric constant of a-domain and that of c-domain by the bulk method using a parallel plate capacitor is difficult. Therefore, at first, we measured the linear dielectric constant of a- and c-domains. The observation images are shown in Fig. 9. In the linear dielectric constant measurements, we measure directly the frequency shifts immediately under the tip. If the high linear dielectric constant area is measured, the frequency shifts low. In Fig. 9, we can see the frequencies in the a-domain areas are lower than those in the

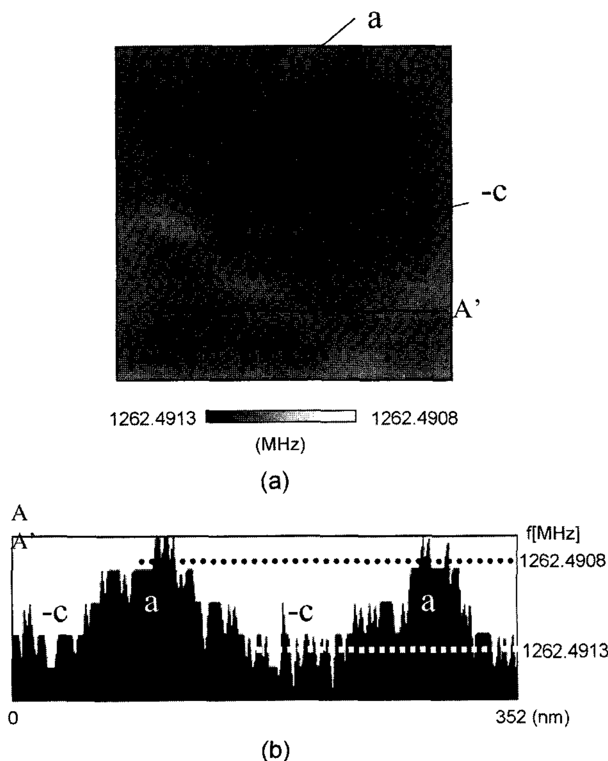

Fig. 9. (a) linear dielectric image of a-c domain in PZT and (b) cross-sectional image along the A-A' line.

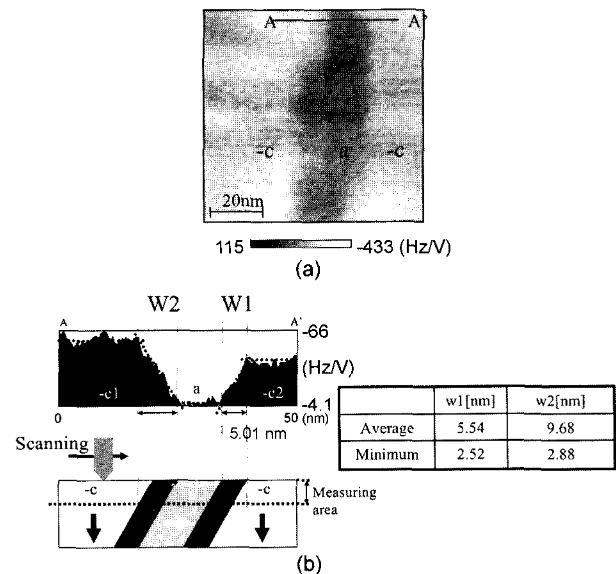

	w1[nm]	w2[nm]
Average	5.54	9.68
Minimum	2.52	2.88

Fig. 10. (a) image of a-c domain wall in PZT and (b) cross-sectional image of a-c domain along the A-A' line.

c-domain areas. So the linear dielectric constant of the a-domain is larger than that of the c-domain. The a-domain was first proven to have a higher linear dielectric constant than that of the c-domain just like a $BaTiO_3$.

Next we observed the domain walls of 90° a-c and 180° c-c domains. Fig. 10(a) is a two-dimensional SNDM image of a-c domain and Fig. 10(b) is the cross-sectional image along the A-A' line in Fig. 10(a). In Fig. 10(b), the thickness of the boundary between a-domain and c1-domain was larger than that between a-domain and c2-domain. Moreover, according to the above-mentioned observation, a-domains have larger linear dielectric constants than c-domains. Therefore, the depth sensitivity at the a-domain becomes thinner than that at the c-domain. As a result, when the c-domain is measured, a signal of thicker area can be obtained than when the a-domain is measured. At the boundary between the c1-domain and the a-domain, the tip senses the a-domain under the c-domain before the tip reaches the real a-c domain boundary. As a result, the signal transition distance between c1-domain and a-domain becomes larger than the thickness of the actual a-c domain boundary. On the other hand, at the boundary between a-domain and c2-domain, the signal shows the change with no influence of c-domain under the a-domain, because the depth sensitivity at the a-domain is thinner than that at the c-domain. As a result, the distance between a-domain and c2-domain can be regarded as the actual a-c domain wall thickness. This wall thickness was measured to be 5.01 nm, as shown in Fig. 10(b). The average thickness and minimum thickness of a-c domain wall were 5.54 nm and 2.52 nm, respectively. The minimum value seems to indicate the ideal domain wall thickness without the influences of the internal electric field or the residual stress stored in the boundary.

In a similar way, we observed the domain wall between the 180° c-c domains. Before observation, we applied +10 V

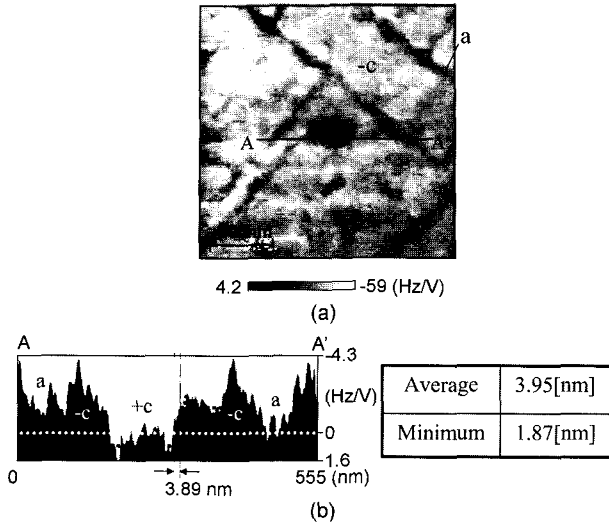

Average	3.95[nm]
Minimum	1.87[nm]

Fig. 11. (a) image of c-c domain wall in PZT and (b) cross-sectional image of c-c domain along the A-A' line.

voltage to the -c domain area to make the +c domain area. Fig. 11(a) shows the two-dimensional SNDM image. The dark area in the center of the image is the +c domain area. Fig. 11(b) is a cross-sectional image along line A-A' shown in Fig. 11(a). The thickness of the c-c domain wall is 3.89 nm in this image. The average thickness and minimum thickness of the c-c domain wall were 3.95 nm and 1.87 nm, respectively. The c-c domain wall had a size of a few unit cells.

In the case of the a-c domain wall, the boundary of a-domain and c-domain is constructed to include lattice strain in order to match the length of the a-axis and the c-axis. On the other hand, in the case of the c-c domain wall, the lattice lengths do not need to match. Therefore, the c-c domain wall does not contain strain, which depends on lattice mismatching. As a result, the c-c domain wall appears to be smaller than the a-c domain wall. Based on the above result, we determined experimentally that the 180° c-c domain wall is thinner than the 90° a-c domain wall.

3. Higher Order Nonlinear Dielectric Microscopy

A higher order nonlinear dielectric microscopy technique with higher lateral and depth resolution than conventional nonlinear dielectric imaging is investigated. The technique is demonstrated to be very useful for observing surface layers of the order of unit cell thickness on ferroelectric materials.

3.1. Theory for Higher Order Nonlinear Dielectric Microscopy

Eq. (2) is a polynomial expansion of the electric displacement D_3 as a function of electric field E_3.

$$D_3 = P_{s3} + \varepsilon_{33}E_3 + \frac{1}{2}\varepsilon_{333}E_3^2 + \frac{1}{6}\varepsilon_{3333}E_3^3 + \frac{1}{24}\varepsilon_{33333}E_3^4 + \cdots \quad (2)$$

Here, ε_{33}, ε_{333}, ε_{3333}, and ε_{33333} correspond to linear and nonlinear dielectric constants and are tensors of rank 2nd, 3rd, 4th, and 5th, respectively. Even-ranked tensors including linear dielectric constant ε_{33} do not change with polarization inversion, whereas the sign of the odd-ranked tensors reverses. Therefore, information regarding polarization can be elucidated by measuring odd-ranked nonlinear dielectric constants such as ε_{333} and ε_{33333}.

Considering the effect up to E^4, the ratio of the alternating variation of capacitance ΔC_s underneath the tip to the static capacitance C_{s0} is given by

$$\frac{\Delta C_s(t)}{C_{s0}} \approx \frac{\varepsilon_{333}}{\varepsilon_{33}}E_p\cos\omega_p t + \frac{1}{4}\frac{\varepsilon_{3333}}{\varepsilon_{33}}E_p^2\cos 2\omega_p t + \frac{1}{24}\frac{\varepsilon_{33333}}{\varepsilon_{33}}E_p^3\cos 3\omega_p t + \cdots \quad (3)$$

This equation shows that the alternating capacitance of different frequencies corresponds to each order of the nonlinear dielectric constant. Signals corresponding to ε_{333}, ε_{3333}, and ε_{33333} were obtained by setting the reference signal of the lock-in amplifier in Fig. 1 to frequency ω_p, $2\omega_p$, and $3\omega_p$ of the applied electric field, respectively.

Next, we consider the resolution of SNDM. From Eq. (2), the resolution of SNDM is found to be a function of electric field E. We note that the electric field under the tip is more highly concentrated with the increase of ε_{33},[19] and the distributions of E^2, E^3, and E^4 fields underneath the tip become much more concentrated in accordance with their power than that of the E field, as shown in Fig. 12. From this figure, we find that higher order nonlinear dielectric imaging has higher resolution than lower order nonlinear dielectric imaging.

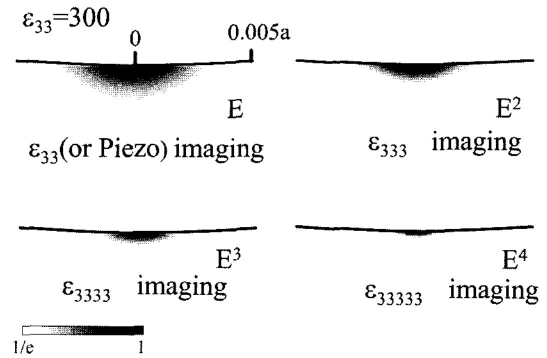

Fig. 12. Distribution of E, E^2, E^3, and E^4 field under the needle tip. a denotes tip radius.

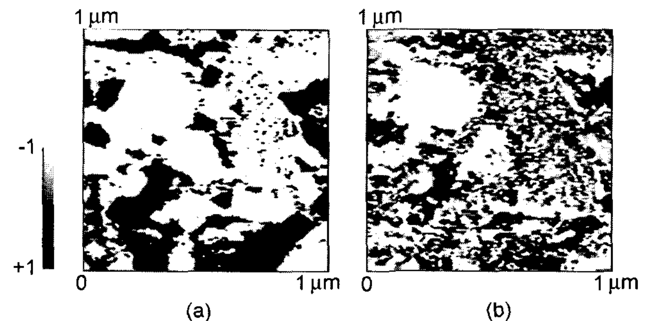

Fig. 13. (a) ε_{333} and (b) ε_{33333} images of PZT thin film.

3.2. Experimental Details of Higher Order Nonlinear Dielectric Microscopy

We experimentally confirmed that ε_{33333} imaging has higher lateral resolution than ε_{333} imaging using a electroconductive cantilever as a tip with a radius of 25 nm. Fig. 13(a) and (b) show ε_{333} and ε_{33333} images of the two-dimensional distribution of lead zirconate titanate PZT thin film. The two images can be correlated, and it is clear that the ε_{33333} image resolves greater detail than ε_{333} image due to the higher lateral and depth resolution.

Next, we investigated the surface layer of periodically poled $LiNbO_3$ (PPLN) by ε_{333}, ε_{3333}, and ε_{33333} imaging. Fig. 14(a) shows ε_{333}, ε_{3333}, and ε_{33333} signals of virgin unpolished PPLN. In this figure, only ε_{333} imaging detects the c-c domain boundary, while ε_{33333} imaging does not. The ε_{3333} signal shows weak peaks at domain boundaries. This is because ε_{3333} and ε_{33333} imaging is affected by the surface paraelectric layer. To prove the existence of a surface paraelectric layer, we polished and measured the PPLN. Fig. 14(b) shows the images of it. In this figure, it is clear that ε_{33333} imaging can detect the c-c domain boundary after removal of the paraelectric layer. Moreover, ε_{3333} imaging can also detect periodic signals, in contrast to our expectation. The nonlinear dielectric signals of a positive area of PPLN are stronger than those of a negative area immediately after polishing, possibly because the negative area is more easily damaged than positive area and has already been covered by a very thin surface paraelectric layer with weak nonlinearity even immediately after polishing. One hour after polishing, we conducted the ε_{333}, ε_{3333}, and ε_{33333} imaging again, and the results are shown in Fig. 14(c). In this figure, the ε_{33333} signal disappears and the ε_{3333} signal becomes flat again, whereas ε_{333} imaging clearly detects the c-c domain boundary (Fig. 14(a)). This implies that the entire surface area of PPLN is covered by the surface paraelectric layer again. From theoretical calculations, on the $LiNbO_3$ substrate, ε_{33333} and ε_{3333} imagings have sensitivities down to 0.75 nm depth and 1.25 nm, respectively, whereas ε_{333} imaging has sensitivity down to 2.75 nm depth when a tip of 25 nm radius is used. Thus, we conclude that the thickness of this surface paraelectric layer ranges between 0.75 nm and 2.75 nm.

From these results, we succeed in observing the growth of the surface layer and we confirm that the negative area of $LiNbO_3$ can be more easily damaged than the positive area.

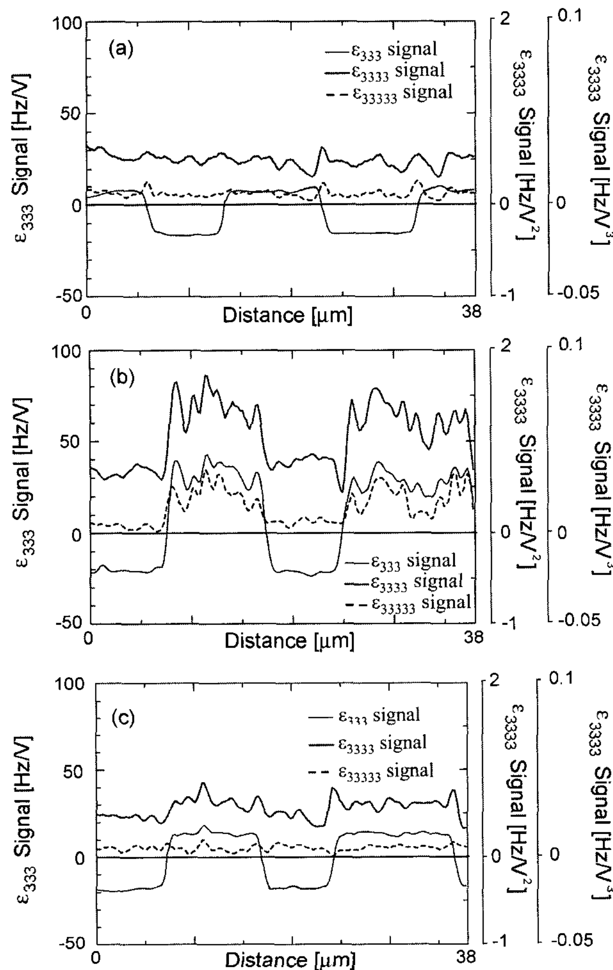

Fig. 14. (a) ε_{333}, ε_{3333}, and ε_{33333} images of virgin PPLN, (b) immediately after polishing, and (c) 1 h after polishing.

4. Ultra High-density Ferroelectric Data Storage Using Scanning Nonlinear Dielectric Microscopy

Ferroelectrics have created considerable interest as promising storage media. Here, an investigation for ultra high-density ferroelectric data storage based on Scanning Nonlinear Dielectric Microscopy (SNDM) was carried out. For the purpose of obtaining the fundamental knowledge of high-density ferroelectric data storage, several experiments of nano-domain formation in Lithium Tantalate ($LiTaO_3$) single crystal were conducted. As a result, very small inverted domain with radius of 6nm was successfully formed in Stoichiometric $LiTaO_3$ (SLT), and besides, domain dot array with areal density of 1.5Tbit/inch^2 was written in Congruent $LiTaO_3$ (CLT).

4.1. SNDM Domain Engineering System

Fig. 15 shows the schematic diagram of SNDM domain engineering system. The probe is composed of a metal-coated conductive cantilever (typical tip radius is 25~nm), an oscillator and a grounded metal ring. Polarity distinction is performed by SNDM technique. On the other hand, writing is performed by applying relatively large voltage pulse to the specimen and locally switching the polarization direction.

4.2. Nano-domain Formation in $LiTaO_3$ Single Crystal

In this study, we selected $LiTaO_3$ single crystal as a recording medium because this material has suitable characteristics as follows:

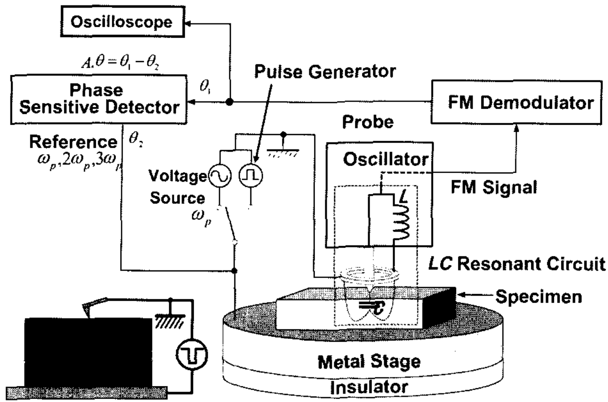

Fig. 15. Schematic diagram of SNDM domain engineering system.

(1) There exist only 180° c-c domains.

(2) It does not possess transition point near room temperature.

(3) High-quality and large single crystal can be fabricated at low cost.

At the present time, two types of $LiTaO_3$ single crystals are widely known; one is stoichiometric $LiTaO_3$ (SLT)[18] and the other is Congruent $LiTaO_3$ (CLT). It is reported that domain inversion characteristics of these crystals are distinctly different each other.[19-21] SLT has few pinning sites of domain switching derived from Li point defects. Therefore, SLT has the characteristics that the coercive field is low and the switching time is short. This means that SLT is favorable for low-power and high-speed writing.

Fig. 16 shows D-E hysteresis of SLT and CLT measured by applying 10 mHz triangular wave voltage, and lower coercive field of SLT compared with that of CLT can be confirmed. On the other hand, CLT has many pinning sites because it is Ta-rich crystal, and it is known that natural domain size of CLT is much smaller than that of SLT. Therefore, we expect that CLT is suitable for higher density storage with smaller domain dots. In the case of forming inverted domain by means of applying voltage to a specimen using a sharp-pointed tip, electric field is highly concentrated just under the tip. So, if the specimen is very thick as compared to the tip radius, large voltage is required for domain switching. Therefore, making thin specimens is very important. In this study, we prepared specimens with thickness of about 100 nm.

Fig. 17 shows SNDM images of typical nano-sized inverted domains formed in a 100 nm thick SLT medium by means of applying voltage pulses with amplitude of 15 V and duration time of (a) 500ns (b) 100 ns (c) 60 ns. From these figures, we found that the area of the domain decreases with decreasing voltage application time.

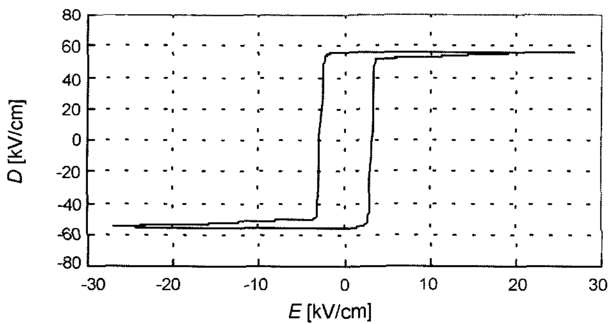

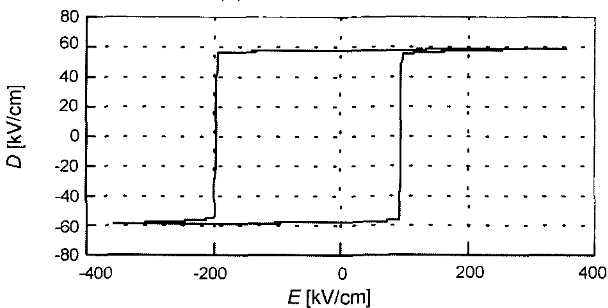

Fig. 16. D-E hysteresis loop of $LiTaO_3$ measured by applying 10 mHz triangular wave voltage.

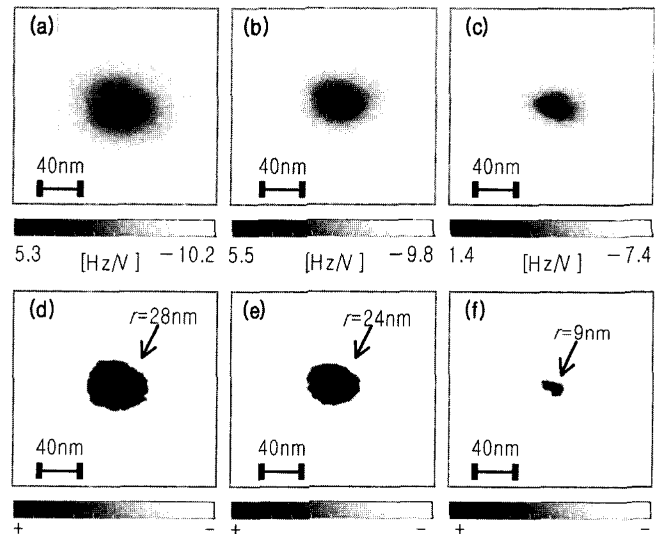

Fig. 17. Images of typical inverted domains formed in SLT by means of applying a voltage pulse with amplitude of 15V and duration time of (a),(d) 500 ns, (b),(e) 100 ns, (c),(f) 60 ns. (a)-(c) Acosθ images, (d)-(f) polarity images.

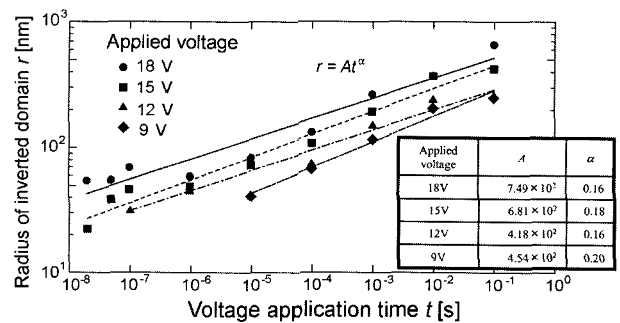

Applied voltage	A	α
18V	7.49×10^2	0.16
15V	6.81×10^2	0.18
12V	4.18×10^2	0.16
9V	4.54×10^2	0.20

Fig. 18. Relationship between the radius of the inverted domain and voltage application time in SLT. Sample thickness is 250 nm.

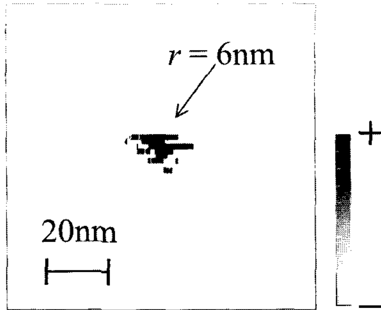

Fig. 19. The smallest inverted domain obtained in this study, which was formed in 100 nm thick SLT by applying 15 V, 60ns pulse.

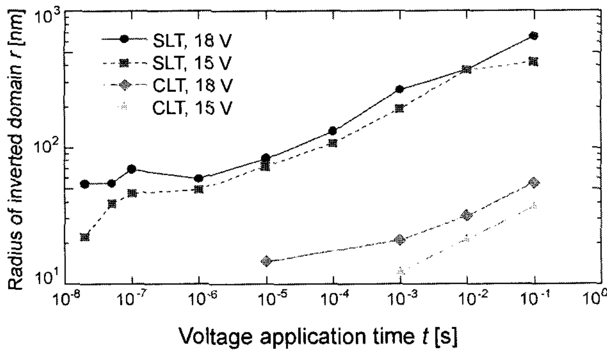

Fig. 20. Relationship between the radius of the inverted domain and voltage application time in SLT and CLT. Sample thickness is 250 nm.

The dependence of domain size on voltage application time is derived from sidewise motion of domain wall. More detailed experimental result with regard to the relationship between the radius of the inverted domain and voltage application time is shown in Fig. 18.

Fig. 19 shows the smallest inverted domain dot obtained in this study. The radius of this domain is 6 nm, which corresponds to storage density of 4Tbit/inch^2 if more than one dot can be formed in close-packed array.

Fig. 20 shows the relationship between the radius of the inverted domain and voltage application time in SLT and CLT. Voltage application time required for forming a certain size of domain in SLT and CLT are different by five to six orders of magnitude. This difference in switching time is derived from the difference in the number of domain pinning sites. Short switching time in SLT is favorable for low-power and high-speed writing. Subsequently, we conducted some experiments of forming any domain shape by means of applying voltage pulses in multipoint while controlling the probe position.

Fig. 21 shows the domain characters 'TOHOKU UNIV.' written in SLT and CLT. The inverted domain in Fig. 21(a) was formed in 150 nm thick SLT by applying 15 V, 100 ns voltage pulses, and the inverted domain in Fig. 21(b) was formed in 70 nm thick CLT by applying 14 V, 10 ms voltage pulses for the left figure and 14 V, 5 ms voltage pulses for the right figure. From these figures, we found that small

(a) SLT (Sample thickness: 150 nm)

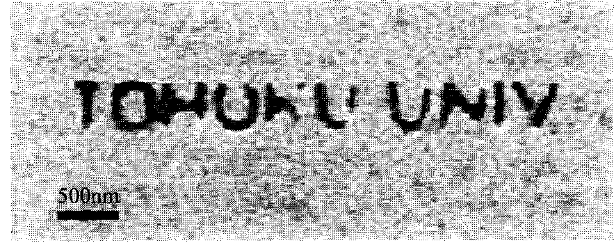

Applied pulse : 15 V, 100 nsec

(b) CLT (Sample thickness: 70 nm)

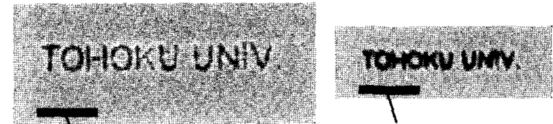

500 nm 500 nm

Applied pulse : 14 V, 10 μsec Applied pulse : 14 V, 5 μsec

Fig. 21. Nano-domain characters 'TOHOKU UNIV.' written in (a) SLT and (b) CLT.

(a)

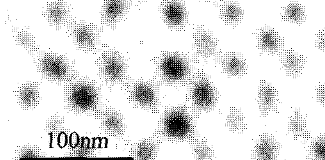

Storage density: 0.62 Tbit/inch^2
Applied voltage: 11 V
Voltage application time: 10 μs
Sample thickness: 70 nm

(b)

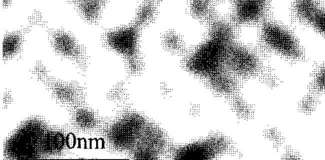

Storage density: 1.10 Tbit/inch^2
Applied voltage: 12 V
Voltage application time: 500 ns
Sample thickness: 70 nm

(c)

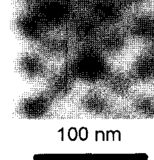

100 nm

Storage density: 1.50 Tbit/inch^2
Applied voltage: 12 V
Voltage application time: 80 ns
Sample thickness: 70 nm

Fig. 22. Images of the inverted domain pattern formed in CLT with density of (a) 0.62Tbit/inch^2, (b) 1.10Tbit/inch^2, and (c) 1.50Tbit/inch^2.

inverted domain pattern was successfully formed in CLT despite of applying relatively long pulses on a thinner sample. This result is vividly reflects that pinning sites derived from lithium nonstoichiometry prevent the sidewise motion of domain walls. Thereby, we verified the feasible storage density using CLT.

Fig. 22 shows images of the inverted domain pattern in CLT with density of (a) 0.62 Tbit/inch^2, (b) 1.10 Tbit/inch^2, (c) 1.50 Tbit/inch^2. These domain patterns were formed by applying voltage pulses with amplitude of (a) 11 V (b), (c) 12 V,

and duration time of (a) 10 μs, (b) 500 ns, and (c) 80 ns. Close-packed dot array composed of positive and negative domain can be seen in these figures.

Although the dots in the 1.50 Tbit/inch^2 array may not be resolvable with sufficient accuracy for practical data storage, this system is fully expected to become practically applicable as a storage system after further refinement. We have thus demonstrated, using a ferroelectric medium and nano-domain engineering, that rewritable bit storage at a data density of more than 1 Tbit/inch^2 is achievable. To the best of our knowledge, this is the highest density reported for rewritable data storage, and is expected to stimulated renewed interest in this approach to next-generation ultra-high-density rewritable electric data storage systems.

5. Conclusions

In this paper, first, a sub-nanometer resolution Scanning Nonlinear Dielectric Microscope (SNDM) for the observation of ferroelectric polarization was described. We also demonstrated that the resolution of SNDM is higher than that of a conventional piezo-response imaging. Using SNDM, we measured the wall thickness of PZT thin film. We also described the theoretical resolution of SNDM. This theoretical result predicted that an atomic scale image can be taken by SNDM.

Next, we reported new SNDM technique detecting higher nonlinear dielectric constants ε_{3333} and ε_{33333}. It is expected that higher order nonlinear dielectric imaging will provide higher lateral and depth resolution. Using this higher order nonlinear dielectric microscopy technique, we successfully investigated the surface layer of ferroelectrics.

Finally, the formation of artificial small inverted domain was reported to demonstrate that SNDM system is very useful as a nano-domain engineering tool. The nano-size domain dots were successfully formed in $LiTaO_3$ single crystal. This means that we can obtain a very high density ferroelectric data storage with the density above 1 Tbits/inch^2.

Therefore, we have concluded that the SNDM is very useful for observing ferroelectric nano domain and local crystal anisotropy of dielectric material with sub-nano meter resolution and also has a quite high potential as a nano-domain engineering tool.

Acknowledgement

We would like to sincerely thank Prof. H. Funakubo of Tokyo Institute of Technology and Prof. R. Ramesh of University of Maryland for supplying the PZT thin film samples.

REFERENCES

1. Y. Cho, A. Kirihara, and T. Saeki, "New Microscope for Measuring the Distribution of Nonlinear Dielectric Properties (in Japanese)", Denshi Joho Tsushin Gakkai Ronbunshi, **J78-C-1** [11] 593-98 (1995).
2. Y. Cho, A. Kirihara, and T. Saeki, "New Microscope for Measuring the Distribution of Nonlinear Dielectric Properties," Electronics and Communication in Japan, Part 2, **79** [6] Scripta Technica, Inc., 68-75 (1996).
3. Y. Cho, A. Kirihara, and T. Saeki, "Scanning Nonlinear Dielectric Microscope," *Rev. Sci. Instrum*, **67** [6] 2297-303 (1996).
4. Y. Cho, S. Atsumi, and K. Nakamura, "Scanning Nonlinear Dielectric Microscope Using a Lumped Constant Resonator Probe and Its Application to Investigation of Ferroelectric Polarization Distributions," *Jpn. J. Appl. Phys.*, **36** [5B] 3152-56 (1997).
5. Y. Cho, S. Kazuta, and K. Matsuura, "Scanning Nonlinear Dielectric Microscopy with Nanometer Resolution," *Appl. Phys. Lett.*, **72** [18] 2833-35 (1999).
6. H. Odagawa and Y. Cho, "Simultaneous Observation of Nano-sized Ferroelectric Domains and Surface Morphology Using Scanning Nonlinear Dielectric Microscopy," *Surf. Sci.*, **463** L621-L25 (2000).
7. H. Odagawa and Y. Cho, "Theoretical and Experimental Study on Nanoscale Ferroelectric Domain Measurement Using Scanning Nonlinear Dielectric Microscopy," *Jpn. J. Appl. Phys.*, **39** [9B] 5719-22 (2000).
8. A. Gruverman, O. Auciello, R. Ramesh, and H. Tokumoto, "Scanning Force Microscopy of Domain Structure in Ferroelectric Thin Films : Imaging and Control," *Nanotechnology*, **8** A38-43 (1997).
9. L. M. Eng, H.-J. Güntherodt, G. A. Schneider, U. Köpke, and J.Muñoz Saldaña, "Nanoscale Reconstruction of Surface Crystallography from Three-dimensional Polarization Distribution in Ferroelectric Barium-titanate Ceramics," *Appl. Phys. Lett.*, **74** [2] 233-35 (1999).
10. Y. Cho, K. Ohara, A. Koike, and H. Odagawa, "New Functions of Scanning Nonlinear Dielectric Microscopy Higher-Order Measurement and Vertical Resolution," *Jpn. J. of Appl. Phys.*, **40** [5B] 3544-48 (2001).
11. K. Ohara and Y. Cho, "Fundamental Study of Surface Layer on Ferroelectrics by Scanning Nonlinear Dielectric Microscopy," *Jpn. J. Appl. Phys.*, **40** [9B] 5833-36 (2001).
12. Y. Cho and K. Ohara, "Higher Order Nonlinear Dielectric Microscopy," *Appl. Phys. Lett.*, **79** [23] 3842-44 (2001).
13. C. S. Ganpule, V. Nagarajan, H. Li, A. S. Ogale, D. E. Steinhauer, S Aggarwal, E. Williams, R. Ramesh, and P. De Wolf, "Role of 90° Domains in Lead Zirconate Titanate Thin Films," *Appl. Phys. Lett.*, **77** [2] 292-94 (2000).
14. Y. Cho, K. Ohara, S. Kazuta, and H. Odagawa, "Theory of Scanning Nonlinear Dielectric Microscopy and Application to Quantitative Evaluation," *J. Eur. Ceram. Soc.*, **21** 2135-39 (2001).
15. H. Odagawa and Y. Cho, "Theoretical and Experimental Study on Nanoscale Ferroelectric Domain Measurement Using Scanning Nonlinear Dielectric Microscopy," *Jpn. J. Appl. Phys.*, **39** [9B] 5719-22 (2000).
16. Y. Ishibashi, "The 90°-wall in the Tetragonal Phase of $BaTiO_3$-type Ferroelectrics," *J. Phys. Soc. Jpn.*, **62** [3], 1044-47 (1993).
17. K. Matsuura, Y. Cho, and H. Odagawa, "Measurement of the Ferroelectric Domain Distributions Using Nonlinear

Dielectric Response and Piezoelectric Response," *Jpn. J. of Appl. Phys.*, **40** [5B] 3534-37 (2001).

18. Y. Furukawa, K. Kitamura, E. Suzuki, and K. Niwa, "Stoichiometric $LiTaO_3$ Single Crystal Growth by Double Crucible Czochralski Method Using Automatic Powder Supply System," *J. Cryst. Growth*, **197** 889-95 (1999).
19. K. Kitamura, Y. Furukawa, K. Niwa, V. Gopalan, and T. E. Mitchell, "Crystal Growth and Low Coercive Field 180° Domain Switching Characteristics of Stoichiometric $LiTaO_3$," *Appl. Phys. Lett.*, **73** [21] 3073-75 (1998).
20. V. Gopalan, T. E. Mitchell, and K. E. Sicakfus, "Switching Kinetics of 180° Domains in Congruent $LiNbO_3$ and $LiTaO_3$ Crystals," *Solid State Commun.*, **109** 111-17 (1999).
21. S. Kim, V. Gopalan, K. Kitamura, and Y. Furukawa," Domain Reversal and Nonstoichiometry in Lithium Tantalate," *J. Appl. Phys.*, **90** [6] 2949-63 (2001).